Journal of the Atmospheric Sciences

Collision fluctuations of lucky droplets with superdroplets

--Manuscript Draft--

Manuscript Number:	JAS-D-20-0371
Full Title:	Collision fluctuations of lucky droplets with superdroplets
Article Type:	Article
Corresponding Author:	Xiang-Yu Li NORDITA Stockholm, SWEDEN
Corresponding Author's Institution:	NORDITA
First Author:	Xiang-Yu Li
Order of Authors:	Xiang-Yu Li
	Bernhard Mehlig
	Gunilla Svensson
	Axel Brandenburg
	Nils Haugen
Abstract:	Direct numerical simulations of collisional aggregation of droplets in atmospheric flows are computation- ally demanding. An alternative is to use a more efficient, yet approximate, model of the collision-coalescence process. The model relies on representing several physical droplets in terms of ‘superdroplets’. Instead of following all droplets, one only tracks collisions between superdroplets and accounts for collisions between physical droplets using a Monte-Carlo algorithm. It was previously shown that this algorithm can faithfully represent mean droplet growth in turbulent aerosols. But an open question is how accurately the superdroplet method accounts for fluctuations in the collisional aggregation process. Such fluctuations are particularly important in dilute suspensions. Even in the absence of turbulence, Poisson fluctuations of collision times in dilute suspensions may result in substantial fluctuations in the growth process, resulting in a broad distribution of growth times to reach a certain droplet size. We quantify the accuracy of the superdroplet method in de- scribing the fluctuating growth history of a larger droplet that settles under the effect of gravity in a quiescent fluid and collides with a dilute suspension of smaller droplets that were initially randomly distributed in space (‘lucky droplet model’). We assess the effect of fluctuations upon the growth history of the lucky droplet and

	compute the distribution of cumulative collision times. The latter is shown to be sensitive enough to detect the subtle increase of fluctuations associated with collisions between multiple lucky droplets. We conclude that the superdroplet algorithm can faithfully represent fluctuations in the coagulation of droplets driven by gravity.
Suggested Reviewers:	Raymond Shaw rashaw@mtu.edu
	Michael Wilkinson m.wilkinson@open.ac.uk
	Alex B. Kostinski kostinsk@mtu.edu
	Wojciech Grabowski grabow@ucar.edu
	Hanna Pawłowska hanna.pawlowska@igf.fuw.edu.pl

Collision fluctuations of lucky droplets with superdroplets

Xiang-Yu Li*

Department of Meteorology and Bolin Centre for Climate Research, Stockholm University, Stockholm, Sweden;

Nordita, KTH Royal Institute of Technology and Stockholm University, 10691 Stockholm, Sweden;

Swedish e-Science Research Centre, www.e-science.se, Stockholm, Sweden;

JILA and Laboratory for Atmospheric and Space Physics, University of Colorado, Boulder, CO 80303, USA

Bernhard Mehlig

Department of Physics, Gothenburg University, 41296 Gothenburg, Sweden

Gunilla Svensson

Department of Meteorology and Bolin Centre for Climate Research, Stockholm University, Stockholm, Sweden;

Swedish e-Science Research Centre, www.e-science.se, Stockholm, Sweden

Axel Brandenburg

Nordita, KTH Royal Institute of Technology and Stockholm University, 10691 Stockholm, Sweden;

JILA and Laboratory for Atmospheric and Space Physics, University of Colorado, Boulder, CO 80303, USA;

Department of Astronomy, Stockholm University, SE-10691 Stockholm, Sweden

Nils E. L. Haugen

SINTEF Energy Research, 7465 Trondheim, Norway;

Department of Energy and Process Engineering, NTNU, 7491 Trondheim, Norway

[*] *Corresponding author address:* Xiang-Yu Li, Department of Meteorology and Bolin Centre for Climate Research, Stockholm University, Stockholm, Sweden

E-mail: xiang.yu.li@su.se, December 17, 2020, Revision: 1.575

ABSTRACT

Direct numerical simulations of collisional aggregation of droplets in atmospheric flows are computationally demanding. An alternative is to use a more efficient, yet approximate, model of the collision-coalescence process. The model relies on representing several physical droplets in terms of 'superdroplets'. Instead of following all droplets, one only tracks collisions between superdroplets and accounts for collisions between physical droplets using a Monte-Carlo algorithm. It was previously shown that this algorithm can faithfully represent mean droplet growth in turbulent aerosols. But an open question is how accurately the superdroplet method accounts for fluctuations in the collisional aggregation process. Such fluctuations are particularly important in dilute suspensions. Even in the absence of turbulence, Poisson fluctuations of collision times in dilute suspensions may result in substantial fluctuations in the growth process, resulting in a broad distribution of growth times to reach a certain droplet size. We quantify the accuracy of the superdroplet method in describing the fluctuating growth history of a larger droplet that settles under the effect of gravity in a quiescent fluid and collides with a dilute suspension of smaller droplets that were initially randomly distributed in space ('lucky droplet model'). We assess the effect of fluctuations upon the growth history of the lucky droplet and compute the distribution of cumulative collision times. The latter is shown to be sensitive enough to detect the subtle increase of fluctuations associated with collisions between multiple lucky droplets. We conclude that the superdroplet algorithm can faithfully represent fluctuations in the coagulation of droplets driven by gravity. To what extent the superdroplet method describes fluctuations of collision histories of droplets in turbulence remains an open question.

1. Introduction

Direct numerical simulations (DNS) have become an essential tool to investigate collisional growth of droplets in turbulence (Onishi et al., 2015; Saito and Gotoh, 2018). The most natural and physical way to analyze collisional growth is to track individual droplets and to record their collisions, one by one. However, DNS of the collision-coalescence process are very challenging, not only when a large number of droplets must be tracked, but also because the flow must be resolved over a large range of time and length scales.

In the past ten years, an alternative way of modeling aerosols has gained popularity. The idea is to combine physical aerosol droplets into 'superdroplets' (Zsom and Dullemond, 2008; Shima et al., 2009). To gain efficiency, one tracks only superdroplet collisions and uses a Monte-Carlo algorithm (Sokal, 1997) to account for collisions between physical droplets. The superdroplet algorithm is used in both the meteorological literature (Andrejczuk et al., 2008; Shima et al., 2009; Andrejczuk et al., 2010; Sölch and Kärcher, 2010; Patterson and Wagner, 2012; Riechelmann et al., 2012; Arabas and Shima, 2013; Naumann and Seifert, 2015, 2016; Jokulsdottir and Archer, 2016; Unterstrasser et al., 2017; Dziekan and Pawlowska, 2017; Li et al., 2017, 2018, 2019, 2020; Sato et al., 2017; Brdar and Seifert, 2018; Hoffmann et al., 2019; Dziekan et al., 2019; Grabowski et al., 2019; Grabowski, 2020), as well as in the astrophysical literature (Zsom and Dullemond, 2008; Ormel et al., 2009; Zsom et al., 2010; Johansen et al., 2012; Johansen et al., 2015; Ros and Johansen, 2013; Drakowska et al., 2014; Kobayashi et al., 2019; Baehr and Klahr, 2019; Ros et al., 2019; Nesvorný et al., 2019; Yang and Zhu, 2020; Poon et al., 2020; Li and Mattsson, 2020). Compared with DNS, the superdroplet method is distinctly more efficient. It has been shown to accurately model average properties of droplet growth in turbulent aerosols. Li et al. (2018) demonstrated, for example, that the mean collision rate obtained using the superdroplet algorithm

agrees with the mean turbulent collision rate (Saffman and Turner, 1956) when the droplets are small.

Less is known about how the superdroplet algorithm represents fluctuations in the collisional aggregation process. Dziekan and Pawlowska (2017) compared the results of the superdroplet algorithm with the predictions of the stochastic coagulation equation of Gillespie (1972) in the context of coalescence of droplets settling in a quiescent fluid. Dziekan and Pawlowska (2017) concluded that the results of the superdroplet algorithm qualitatively agree with what Kostinski and Shaw (2005) called the lucky droplet model (LDM). To assess the importance of fluctuations, Dziekan and Pawlowska (2017) computed the time $t_{10\%}$, after which 10% of the droplets have reached a radius of $40\,\mu$m. In agreement with earlier Lagrangian simulations of Onishi et al. (2015), which did not employ the superdroplet algorithm, they found that the difference in $t_{10\%}$ between their superdroplet simulations and the stochastic model of (Gillespie, 1972) decreases with the square root of the number of droplets, provided that there are no more than about nine droplets per superdroplet. When the number of droplets per superdroplet is larger, a residual error remains which the authors attribute to artificial correlations between different droplet sizes. We return to this question in the discussion of the present paper, where we tentatively associate their findings with the occurrence of several large (lucky) droplets that grew from the finite tail of their initial droplet distribution.

The role of fluctuations is particularly important in dilute systems, where rare extreme events may substantially broaden the droplet-size distribution. This is well captured by the LDM, which was first proposed by Telford (1955), and more recently quantitatively analyzed by Kostinski and Shaw (2005). The model describes one large droplet (twice the mass of $10\,\mu$m-sized droplets in radius) settling through a dilute suspension of smaller droplets. The collision times between the larger droplets (the lucky droplet) and the smaller ones are exponentially distributed, leading

to substantial fluctuations in the growth history of the lucky droplet. Wilkinson (2016) derived analytic expressions for the distribution of the cumulative distribution time using large-deviation theory.

The goal of the present paper is to investigate how accurately the superdroplet algorithm represents fluctuations in the collisional growth history of settling droplets in a quiescent fluid. Unlike the work of Dziekan and Pawlowska (2017), we use here the LDM. We record growth histories of the larger droplet in an ensemble of different realizations of identical smaller droplets that were initially randomly distributed in a quiescent fluid. We show that the superdroplet method accurately describes the fluctuations of growth histories of the lucky droplet in an ensemble of simulations. In its simplest form, the LDM assumes that the lucky droplet is large compared with the background droplets so that the radius of those smaller droplets can be neglected in the geometrical collision cross section and collision velocities. Since fluctuations early on in the growth history are most important (Kostinski and Shaw, 2005; Wilkinson, 2016), this can make a certain difference in the distribution of the times T it takes for the lucky droplet to grow to a certain size. Third, since the small droplets are initially randomly distributed, their local number density fluctuates. Lucky droplets can grow most quickly where the local number density of small droplets happens to be large.

The remainder of this paper is organized as follows. In Sec. 2 we describe the superdroplet method and highlight differences between different implementations used in the literature (Shima et al., 2009; Johansen et al., 2012; Li et al., 2017). Section 3 summarizes the LDM, the setup of our superdroplet simulations, and how we measure fluctuations of growth histories. Section 4 summarizes the results of our superdroplet simulations. We conclude in Sec. 6.

2. Method

a. Superdroplet algorithm

Superdroplet algorithms represent several physical droplets in terms of one superdroplet. All droplets in superdroplet i are assumed to have the same material density ρ_{d}, the same radius r_i, the same velocity v_i, and reside in a volume around the same position x_i. The index i labeling the superdroplets ranges from 1 to N_{s} (Table 1). The hydrodynamic force is modeled using Stokes law.

The equation of motion for the position $\boldsymbol{x}_i$ and velocity $\boldsymbol{v}_i$ of superdroplet i reads:

$$\frac{\mathrm{d}\boldsymbol{x}_i}{\mathrm{d}t} = \boldsymbol{v}_i\,, \quad \frac{\mathrm{d}\boldsymbol{v}_i}{\mathrm{d}t} = -\frac{\boldsymbol{v}_i}{\tau_i} + \boldsymbol{g}\,. \tag{1}$$

Here $\boldsymbol{g}$ is the gravitational acceleration,

$$\tau_i = 2\rho_{\mathrm{d}} r_i^2 / 9\rho\nu \tag{2}$$

is the droplet response (or Stokes) time attributed to the superdroplet, and ρ is the mass density of the airflow.

Droplet collisions are represented by collisions of superdroplets (Shima et al., 2009; Johansen et al., 2012; Li et al., 2017), as mentioned above. When two superdroplets collide, a Monte-Carlo scheme is used to determine which pairs of droplets collide. It is assumed that two droplets in either of the superdroplets (with indices i and j) collide with probability

$$p_{ij} = \lambda_{ij}\delta t\,, \tag{3}$$

where δt is the integration time step. A collision happens when $p_{ij} < \eta$, where $0 \leq \eta \leq 1$ is a uniformly distributed random number. To avoid a probability larger than unity, we limit the integration step through the condition $\delta t < 1/\lambda_{ij}$. The collision rate is

$$\lambda_{ij} = \pi \left(r_i + r_j\right)^2 |\boldsymbol{v}_i - \boldsymbol{v}_j| E_{ij} N_{\mathrm{p/s}} / \delta x^3\,, \tag{4}$$

where E_{ij} is the collision efficiency, $N_{\mathrm{p/s}}$ is the larger initial number of droplets per superdroplet i or j (Table 1), and δx^3 is the volume assigned to the superdroplet. To facilitate the comparison with the earlier work, we assume $E_{ij} = 1$ for most of our models.

What happens when two superdroplets collide? To write down the rules, we denote the number of droplets in superdroplet i by $N^i_{\mathrm{p/s}}$, while $N^j_{\mathrm{p/s}}$ is the number of droplets in superdroplet j. M_i and M_j are the corresponding droplet masses. The collision scheme suggested by Shima et al. (2009) amounts to the following rule. To ensure mass conservation between superdroplets i and j, when $N^j_{\mathrm{p/s}} > N^i_{\mathrm{p/s}}$, droplet numbers and masses are updated such that

$$N^i_{\mathrm{p/s}} \to N^i_{\mathrm{p/s}}\,, \quad N^j_{\mathrm{p/s}} \to N^j_{\mathrm{p/s}} - N^i_{\mathrm{p/s}}\,, \tag{5}$$
$$M_i \to M_i + M_j\,, \quad M_j \to M_j\,.$$

When $N^j_{\mathrm{p/s}} < N^i_{\mathrm{p/s}}$, the update rule is also given by equation (5), but with indices i and j exchanged. In other words, the number of droplets in the smaller superdroplet remains unchanged (and their masses are increased), while that in the larger one is reduced by the amount of droplets that have collided with all the droplets of the smaller superdroplet (and their masses remain unchanged). This is illustrated in Figure 1. To ensure momentum conservation during the collision, the momenta of droplets in the two superdroplets are updated as

$$\boldsymbol{v}_i M_i \to \boldsymbol{v}_i M_i + \boldsymbol{v}_j M_j\,,$$
$$\boldsymbol{v}_j M_j \to \boldsymbol{v}_j M_j\,, \tag{6}$$

after a collision of superdroplets. Finally, when $N^i_{\mathrm{p/s}} = N^j_{\mathrm{p/s}}$, droplet numbers and masses are updated as

$$N^i_{\mathrm{p/s}} \to N^i_{\mathrm{p/s}}/2\,, \quad N^j_{\mathrm{p/s}} \to N^j_{\mathrm{p/s}}/2\,, \tag{7}$$
$$M_i \to M_i + M_j\,, \quad M_j \to M_i + M_j\,.$$

The scheme illustrated in Figure 1 does not automatically prevent fractional numbers of droplets per superdroplet. It is then assumed that, when two superdroplets with less than one physical droplet collide, the superdroplet containing the smaller physical droplet is removed from the computational domain after the collision.

b. Numerical setup

In our superdroplet simulations, we consider droplets of radius $10\,\mu$m, randomly distributed in space, together with one droplet of twice the mass and radius $2^{1/3} \times 10\,\mu\text{m} = 12.6\,\mu$m. The larger droplet has a higher settling speed than the $10\,\mu$m droplets and sweeps them up through collision and coalescence. Since the flow is not disturbed by the particles, we neglect two-way coupling. For each simulation, we track the growth history of the larger droplet until it reaches $50\,\mu$m in radius and record the time T it takes to grow to that size.

In the superdroplet algorithm, one usually takes $N_{\mathrm{p/s}} \gg 1$, which implies that the actual number of lucky droplets is also more than one. This was not intended in the original formulation of the lucky droplet model (Telford, 1955; Kostinski and Shaw, 2005; Wilkinson, 2016) and could allow the number of superdroplets with heavier (lucky) droplets, $N_{\mathrm{s}}^{(\mathrm{luck})}$, to become larger than unity. This would manifest itself in the growth history of the lucky droplets through an increase by more than the mass of a background droplet. We refer to this as "jumps". Let us therefore now discuss the conditions under which this would happen and denote the values of $N_{\mathrm{p/s}}$ for the lucky and background droplets by $N_{\mathrm{p/s}}^{(\mathrm{luck})}$ and $N_{\mathrm{p/s}}^{(\mathrm{back})}$, respectively. First, for $N_{\mathrm{p/s}}^{(\mathrm{luck})} = N_{\mathrm{p/s}}^{(\mathrm{back})}$, the masses of both lucky and background droplets can increase, provided their values of $N_{\mathrm{p/s}}$ are above unity; see Figure 1(c). Second, even if $N_{\mathrm{p/s}}^{(\mathrm{luck})} < N_{\mathrm{p/s}}^{(\mathrm{back})}$ initially, new lucky superdroplets could in principle emerge when the *same* two superdroplets collide with each other multiple times. This can happen for two reasons. First, the use of periodic boundary conditions for the superdroplets

(i.e., in the vertical direction in our laminar model with gravity). Second, two superdroplets can remain at the same location (corresponding to the same meshpoint of the Eulerian grid for the fluid) during subsequent time steps. (Our time step must be less than the time for a superdroplet to fall from one meshpoint to the next.) Looking at Figure 1, we see that $N_{\mathrm{p/s}}^{(\mathrm{back})}$ can then decrease after each collision and potentially become equal to or drop below the value of $N_{\mathrm{p/s}}^{(\mathrm{luck})}$. This becomes exceedingly unlikely if initially $N_{\mathrm{p/s}}^{(\mathrm{back})} \gg N_{\mathrm{p/s}}^{(\mathrm{luck})}$, but it is not completely impossible, unless $N_{\mathrm{p/s}}^{(\mathrm{luck})}$ is chosen initially to be unity.

The initial value of $N_{\mathrm{p/s}}^{(\mathrm{back})}$ can in principle also be chosen to be unity. Although such a case will indeed be considered here, it would defeat the purpose and computational advantage of the superdroplet algorithm. Therefore, we also consider the case $N_{\mathrm{p/s}}^{(\mathrm{back})} \gg N_{\mathrm{p/s}}^{(\mathrm{luck})}$. As already mentioned, jumps are impossible if $N_{\mathrm{p/s}}^{(\mathrm{luck})}$ is unity.

Unless otherwise specified, the viscosity equals $\nu = 10^{-5}\,\mathrm{m^2\,s^{-1}}$ and the initial droplet number density is set to $n = 10^8\,\mathrm{m^{-3}}$. For orientation, we note that the speed of the lucky droplet prior to the first collision is about $3.5\,\mathrm{cm\,s^{-1}}$, the average time to the first collision is 490 s, and thus, it falls over a distance of about 17 m before it collides.

The superdroplet algorithm is usually applied to three-dimensional (3-D) simulations. If there is no horizontal mixing, one can consider one-dimensional (1-D) simulations. Moreover, we are only interested in the column in which the lucky droplet resides. In 3-D, however, the number density of the $10\,\mu$m droplets beneath the lucky one is in general not the same as the mean number density of the whole domain. This leads to yet another element of randomness that we shall consider in this paper by studying the difference between 1-D and 3-D simulations, and fluctuations of the number density between columns.

3. Lucky-droplet models

a. Basic idea

In its simplest form, the LDM describes the collisional growth of a larger droplet that settles through a quiescent fluid and collides with smaller monodisperse droplets, that were initially randomly distributed in space. This corresponds to the setup described in the previous section. We begin by recalling the main conclusions of Kostinski and Shaw (2005). Initially, the lucky droplet has a radius corresponding to a volume twice that of the background droplets, whose radius was assumed to be $r_1 = 10\,\mu$m. Therefore, its initial radius is $r_2 = 2^{1/3} r_1 = 12.6\,\mu$m. After the kth collision step with smaller droplets, it increases as

$$r_k \sim r_1 k^{1/3}. \tag{8}$$

Fluctuations in the length of the time intervals t_k between collision $k-1$ and k give rise to fluctuating growth histories of the larger droplet. These fluctuations are quantified by the distribution of the cumulative time

$$T = \sum_{k=2}^{125} t_k, \tag{9}$$

corresponding to 124 collisions needed for the lucky droplet to grow from $12.6\,\mu$m to $50\,\mu$m. The time intervals t_k between successive collisions are drawn from an exponential distribution with a probability $p_k(t_k) = \lambda_k \exp(-\lambda_k t_k)$. The rates λ_k depend on the differential settling velocity $|\boldsymbol{v}_k - \boldsymbol{v}_1|$ between the colliding droplets through equations (3) and (4). Here, however, the background droplets have always the radius r_1, so $\lambda_k \equiv \lambda_{k1}$, i.e., the second index is here dropped, because it is always 1. Likewise, we also drop the second index on the collision efficiency, i.e., $E_k \equiv E_{k1}$.

It is well known that $E_k \ll 1$ (Pruppacher and Klett, 1997). However, as an idealization, it is instructive to assume $E_k = 1$ for all k, so the collision rate (4) can be approximated as $\lambda_k \sim r_k^4$ which is permissible when $r_k \gg r_1$. It follows that, in terms of the number of collisions k, the

collision frequency is

$$\lambda_k = \lambda_* k^{4/3}, \tag{10}$$

where $\lambda_* = (2\pi/9)(\rho_\mathrm{d}/\rho)(gn/\nu)r_1^4$, and n is the number density of the $10\,\mu$m background droplets. This is essentially the model of Kostinski and Shaw (2005) and Wilkinson (2016), except that they also assumed $E_k \neq 1$. They pointed out that, early on, i.e., for small k, λ_k is small and therefore the mean collision time λ_k^{-1} is long. The actual time until the first collision can then be very long, but it can also be very short, depending on fluctuations. Therefore, at early times, fluctuations have a large impact on the cumulative collision time.

b. The effects of various approximations

We now discuss the significance of the various approximations being employed in the LDM. To relax the approximations made in equation (10), we now write it in the form

$$\lambda_k = \lambda_* E_k r_\mathrm{A}^2(r_k) r_\mathrm{B}^2(r_k)/r_1^4 \quad (k \geq 2), \tag{11}$$

where

$$r_\mathrm{A}^2 = (r_k + r_1)^2, \quad r_\mathrm{B}^2 = r_k^2 - r_1^2 \tag{12}$$

would correspond to the expression equation (4) used in the superdroplet model. In equation (10), however, it was assumed that $r_\mathrm{A} = r_\mathrm{B} = r_k$. To distinguish this approximation from the form used in equation (11), we denote that case by writing symbolically "$r_\mathrm{A} \neq r_k \neq r_\mathrm{B}$"; see Figure 2.

In equation (12), we have introduced r_A and r_B to study the effect of relaxing the assumption $r_\mathrm{A} = r_\mathrm{B} = r_k$, made in simplifying implementations of the LDM. Both of these assumptions are justified at late times when the lucky droplet has become large compared to the smaller ones, but not early on, when the size difference is moderate.

By comparison, in mean-field theory (MFT), one assumes deterministic collision times that are given by $t_k = \lambda_k^{-1}$. In Figure 3 we demonstrate the effect of the contributions from r_A and r_B on the mean cumulative collision time in the corresponding MFT,

$$T_k^{\mathrm{MFT}} = \sum_{k'=2}^{k} t_{k'}^{\mathrm{MFT}}, \tag{13}$$

where

$$t_k^{\mathrm{MFT}} = \lambda_k^{-1} \tag{14}$$

are the inverse of the mean collision rates. In the right-hand panel, we also see that the contributions to the two correction factors r^2/r_A^2 and r^2/r_B^2 have opposite trends, which leads to partial cancelation in their product.

As already stated, we are interested in the distribution of cumulative collision times, $P(T)$. In Figure 4 we show a comparison of the distribution of cumulative collision times for various representations of r_k. The physically correct model is where $r_\mathrm{A} \neq r_k \neq r_\mathrm{B}$ (black line). To demonstrate the sensitivity of $P(T)$ to changes in the representation of r_k, we show the result for the approximations $r_\mathrm{A} = r_k = r_\mathrm{B}$ (red line) and $r_\mathrm{A} \neq r_k = r_\mathrm{B}$ (blue line). The $P(T)$ curve is also sensitive to changes in the collision efficiency late in the evolution. To demonstrate this, we assume $E_k \propto r_k^2$ when $r_k \geq r_*$ (Lamb and Verlinde, 2011). To ensure that $E_k \leq 1$, we assume

$$E_k = E_* \max\left(1, (r/r_*)^2\right), \tag{15}$$

where $E_* \leq 1$ has been introduced to ensure $E_k \leq 1$. However, the normalized $P(T)$ curves are independent of the choice of the value of E_*. In Figure 5, we show the results for $r_\mathrm{A} \neq r_k \neq r_\mathrm{B}$ using $r_* = 40\,\mu$m and $30\,\mu$m (red and blue lines, respectively) and compare with the case $E_k = $ const. The more extreme cases with $r_* = 20\,\mu$m and $10\,\mu$m are shown as gray lines. The latter is similar to the case $\lambda_k \sim r_k^6$ considered by Kostinski and Shaw (2005) and Wilkinson (2016).

As anticipated by Kostinski and Shaw (2005), $P(T)$ can be approximated by a lognormal distribution in all cases, as can be seen from the approximately inverted parabolic shape in the double-logarithmic representation in Figure 4. When $r_A = r_k = r_B$, or only $r_k = r_B$, the $P(T)$ curves exhibit smaller widths. By contrast, when the collision efficiency becomes quadratic later on (when $r > r_* \equiv 30\,\mu$m or $40\,\mu$m), the $P(T)$ curves have larger widths; see Figure 5.

To quantify the shape of $P(T)$, we give in Table 2 the average of $X \equiv \ln(T/\langle T\rangle)$, its standard deviation $\sigma = \langle x^2\rangle^{1/2}$, where $x \equiv X - \langle X\rangle$, its skewness skew $X = \langle x^3\rangle/\sigma^3$, and its kurtosis kurt $X = \langle x^4\rangle/\sigma^4$. The main conclusion that can be drawn form the investigation mentioned above is that it does not result in any significant error to assume $r_k \gg r_1$. The value of σ is only about 10% smaller if $r_A = r_k = r_B$ is used (compare the red dashed and black solid lines in Figure 4). This is because the two inaccuracies introduced by r_A and r_B almost cancel each other. When $r_* = 40\,\mu$m or $30\,\mu$m, for example, the values of σ increase by 3% and 15%, respectively; see Table 2, where we also list the corresponding values of $T_k^{\rm MFT}$.

A straightforward extension of the LDM is to take horizontal variations in the local column density into account. Those are always present for any random initial conditions, but could be larger for turbulent systems, regardless of the droplet speeds. Indeed, in our 3-D superdroplet simulations, large droplets can fall in different vertical columns that contain different numbers of small droplets, a consequence of the fact that the small droplets are initially randomly distributed. To describe the results of our 3-D simulations, it is necessary to solve for an ensemble of columns with different number density of the $10\,\mu$m background droplets and compute the distribution of cumulative collision times. We present a corresponding comparison with our superdroplet model at the end of this paper.

c. Relation to the superdroplet algorithm

To understand the nature of the superdroplet algorithm, and why it captures the lucky droplet problem accurately, it is important to realize that the superdroplet algorithm is actually a combination of two separate approaches, each of which turns out to be able to reproduce the lucky droplet problem to high precision. In principle, we can distinguish four different approaches to obtaining the collision time interval t_k. In the LDM, t_k was taken from an exponential distribution of random numbers (approach I). Another approach is to use a randomly distributed set of $10\,\mu$m background droplets and then to solve for the collisions between the lucky droplets and the background explicitly (approach II). A third approach is to use a Monte-Carlo method to solve for the time evolution to decide whether at any time there is a collision or not (approach III). This is actually what is done within each grid cell in the superdroplet algorithm; see equations (3) and (4). The fourth approach is the superdroplet algorithm discussed extensively in section 2a (approach IV). It is essentially a combination of approaches II and III. We have compared all four approaches and found that they all give very similar results. In the following, we describe approaches II and III in more detail, before focussing on approach IV in section 4.

d. Solving for the collisions explicitly

A more realistic method (approach II) is to compute random realizations of droplet positions in a tall box of size $L_\mathrm{h}^2 \times L_z$, where L_h and L_z are the horizontal and vertical extents, respectively. We position the lucky droplet in the middle of the top plane of the box. Collisions are only possible within a vertical cylinder of radius $r_k + r_1$ below the lucky droplet. Next, we calculate the distance Δz to the first collision partner within the cylinder. We assume that both droplets reach their terminal velocity well before the collision. This is an excellent approximation for dilute systems such as clouds, because the droplet response time τ_k of equation (2) is much shorter than the mean

collision time. We can then assume the relative velocity between the two as given by the difference of their terminal velocities as

$$\Delta v_k = (\tau_k - \tau_1)\, g. \tag{16}$$

The time until the first collision is then given by $t_2 = \Delta z/\Delta v_2$. This collision results in the lucky droplet having increased its volume by that of the $10\,\mu$m droplet. Correspondingly, the radius of the vertical cylinder of collision partners is also increased. We then search for the next collision partner beneath the position of the first collision, using still the original realization of $10\,\mu$m droplets. We continue this procedure until the lucky droplet reaches a radius of $50\,\mu$m.

e. The Monte-Carlo method to compute t_k

In the Monte-Carlo method (approach III) we choose a time step δt and step forward in time. As in the superdroplet algorithm, the probability of a collision is given by $p_k = \lambda_k \delta t$; see equation (3). We continue until a radius of $50\,\mu$m is reached.

Approach III also allows us to study the effects of jumps in the droplet size by allowing for several lucky droplets at the same time and specifying their collision probability appropriately. These will then be able to interact not only with the $10\,\mu$m background droplets, but they can also collide among themselves, which causes the jumps. We will include this effect into the LDM and compare with the results of the superdroplet algorithm.

4. Results

a. Agreement with the LDM

We now want to determine to what extent the fluctuations are correctly represented by the superdroplet algorithm. For this purpose, we now demonstrate the degree of quantitative agreement between the LDM and the corresponding solution with the superdroplet algorithm. This is done by

tracking the growth history of each lucky droplet. As the first few collisions determine the course of the formation of larger droplets, we also use the distribution $P(T)$ of cumulative collision times T. We perform N_{real} superdroplet simulations with different random seeds using $N_{\mathrm{p/s}} = 1$.

We begin by looking at growth histories for many individual realizations obtained from the superdroplet simulation. Figure 6 shows an ensemble of growth histories (thin gray lines) obtained from $N_{\mathrm{real}} \approx 10^3$ independent simulations, as described above. The times between collisions are random, leading to a distribution of cumulative growth times to reach $50\,\mu$m. Also shown is the mean growth curve (thick black line), obtained by averaging the time at fixed radii r. This figure demonstrates that the fluctuations are substantial. We also see that large fluctuations relative to the average time are rare.

To quantify the effect of fluctuations from all realizations, we now consider the corresponding $P(T)$. It is normalized such that $\int P(T)\,\mathrm{d}T = 1$ and is shown in Figure 7, where we have divided T by its average, $\langle T \rangle \equiv \int_0^\infty T P(T)\,\mathrm{d}T$. We recall that $N_{\mathrm{p/s}} = 1$ for our superdroplet simulation in Figure 7. However, a simulation with $N_{\mathrm{p/s}} = 50$ yields almost the same result; see Appendix A1.

The comparison between LDM and the superdroplet algorithm shows small differences. The width of the $P(T)$ curve is slightly larger in the LDM than in the superdroplet simulations. This suggests that the fluctuations, which are at the heart of the LDM, are slightly underrepresented in the superdroplet algorithm.

In the following, we discuss how our conclusions relate to those of earlier work. We then discuss a number of additional factors that can modify the results (jumps in r or the effects of 3-D, for example). Those additional factors can also be taken into account in the LDM. Even in those cases, it turns out that the differences between the LDM and the superdroplet algorithm are small.

b. The occurrence of jumps

One of the pronounced features in our superdroplet simulations with $N_{\mathrm{p/s}} > 1$ is the possibility of jumps. We see examples in Figure 8 where $N_{\mathrm{p/s}}^{(\mathrm{luck})} = N_{\mathrm{p/s}}^{(\mathrm{back})} = 2$ and the jumps are visualized by the red vertical lines. Those jumps are caused by the coagulation of the lucky droplet with droplets of radii larger than $10\,\mu$m that were the result of other lucky droplets in the simulations. What is the effect of these jumps? Could they be responsible for the behavior found by Dziekan and Pawlowska (2017) that the difference in their $t_{10\%}$ between the numerical and theoretical calculation decreases with the square root of the number of physical droplets, as discussed in Sec. 1?

It is clear that those jumps occur only at late times when there has been enough time to grow several more lucky droplets. Because the collision times are so short at late times, the jumps are expected to be almost insignificant. To quantify this, it is convenient to use approach III, where we allow for $N_{\mathrm{p}}^{(\mathrm{luck})} = 3$ superdroplets simultaneously. They can grow through collisions with the $10\,\mu$m background droplets and through mutual collisions between lucky droplets. The collision rate between lucky droplets i and j is, analogously to equation (11), given by

$$\lambda_{ij}^{(\mathrm{luck})} = \pi \left(r_i + r_j\right)^2 |v_i - v_j|\, n_{\mathrm{luck}}, \tag{17}$$

where $n_{\mathrm{luck}} = \varepsilon n / N_{\mathrm{p}}^{(\mathrm{luck})}$ with ε being the ratio of the physical number of lucky droplets, $N_{\mathrm{p}}^{(\mathrm{luck})}$, to the physical number of background droplets, $N_{\mathrm{p}}^{(\mathrm{back})}$, i.e.,

$$\varepsilon = \frac{N_{\mathrm{p}}^{(\mathrm{luck})}}{N_{\mathrm{p}}^{(\mathrm{back})}} = \frac{N_{\mathrm{p/s}}^{(\mathrm{luck})} N_{\mathrm{s}}^{(\mathrm{luck})}}{N_{\mathrm{p/s}}^{(\mathrm{back})} N_{\mathrm{s}}^{(\mathrm{back})}}. \tag{18}$$

In the first case, where $N_{\mathrm{p/s}}^{(\mathrm{luck})} = N_{\mathrm{p/s}}^{(\mathrm{back})} \equiv N_{\mathrm{p/s}} = 1$ (see Figure 6), we used $N_{\mathrm{s}} = 256$ superdroplets, of which one contained the lucky droplet, so $N_{\mathrm{s}}^{(\mathrm{luck})} = 1$, and the other 255 superdroplets contained a $10\,\mu$m background droplet each. In our superdroplet solution, the ratio was therefore

$\varepsilon = 1/255 = 0.004$. Using Approach III, however, ε enters simply as an extra factor in the collision probability between different lucky droplets; see section 3e. The effect on $P(T)$ is shown in Figure 9, where we present the cumulative collision times for models with three values of ε using approach II. We see that this model does indeed have the same cumulative distribution function as with approach III, so the effect of jumps is very small (compare the black solid and the red dashed lines of Figure 9). More significant departures due to jumps can be seen in $P(T)$ when $\varepsilon = 0.02$ and larger.

The jumps in the growth histories cause the droplets to grow faster. As expected, however, the jumps do not have a noticeable effect upon $P(T)$ in the superdroplet simulations we conducted; see Figure 10. By comparing $P(T)$ for $N_{\mathrm{p/s}}^{(\mathrm{back})} = 40$ (blue crosses in Figure 10) with that for $N_{\mathrm{p/s}}^{(\mathrm{back})} = 2$ (black circles), while keeping $N_{\mathrm{p/s}}^{(\mathrm{luck})} = 2$ in both cases, hardly any jumps occur and the lucky droplet result remains equally accurate.

For larger values of ε, jumps occur much earlier, as can be seen from Figure 11, where we show 30 growth curves for the cases $\varepsilon = 0.004$, which is relevant to the simulations of Figure 7, as well as $\varepsilon = 0.02$, and 0.05. We also see that for large values of ε, the width in the distribution of arrival times is broader and that both shorter and longer times are possible. This suggests that the reason for the finite residual error in the values of $t_{10\%}$ found by Dziekan and Pawlowska (2017) for $N_{\mathrm{p/s}} > 9$ could indeed be due to jumps. In our superdroplet simulations, by contrast, jumps cannot occur when $N_{\mathrm{p/s}} = 1$ or $N_{\mathrm{p/s}}^{(\mathrm{back})} \gg N_{\mathrm{p/s}}^{(\mathrm{luck})}$.

c. The two aspects of randomness

Let us now quantify the departure that is caused by the use of the Monte-Carlo collision scheme. To do this, we need to assess the effects of randomness introduced through equations (3) and (4)

on the one hand and the random distribution of the $10\,\mu$m background droplets on the other. Both aspects enter in the superdroplet algorithm.

We recall that in approach II, fluctuations originate solely from the random distribution of the $10\,\mu$m background droplets. In approach III, on the other hand, fluctuations originate solely from the Monte-Carlo collision scheme. By contrast, the LDM is different from either of the two, because it just uses the exponential distribution of the collision time intervals, which is indirectly reproduced by the random initial droplet distribution in approach II and by the Monte-Carlo scheme in approach III.

In Figure 12, we compare approaches I, II, and III. The differences between them are very minor, and also the first few moments are essentially the same; see Table 3. We thus see good agreement between the different approaches. This suggests that the fluctuations introduced through random droplet positions is not crucial and that it can be substituted by the fluctuations of the Monte-Carlo scheme alone.

It is worth noting that we have been able to perform 10^8 realizations with Approaches II and III, and 10^{10} realizations with Approach I, while in the superdroplet algorithm (Approach IV), we have only been able to run 10^3 realizations. This may be the reason why fluctuations appear to be slightly underrepresented in the superdroplet algorithm. Nevertheless, the agreement between the LDM and the superdroplet simulations demonstrates that the superdroplet approach does not contain mean-field elements. This can be further evidenced by the fact that the results of Approaches II and III agree perfectly with those of Approach I, and the superdroplet approach is just the combination of Approaches II and III.

d. The effects of fluctuations in 3-D simulations

One might have expected that a 3-D simulation could be more realistic and perhaps more accurate than a 1-D simulation. In Figure 13 we compare the resulting $P(T)$ for 3-D and 1-D cases. The result is surprising in that the $P(T)$ curves from the two cases are rather different. The $P(T)$ curve from the 1-D case agrees well with the LDM using approaches I–III. In the 3D case, the fluctuations appear to be vastly exaggerated, similarly to the blue line in Figure 4. This will be discussed next.

An important difference between 1-D and 3-D is the fact that in 3-D, we accumulate statistics for lucky droplets that fall through vertical columns whose mean droplet number density fluctuates from one column to another. These fluctuations lead to a broadening of $P(T)$, but it is a priori not evident that this explains the 3-D results quantitatively.

In Figure 14, we compare the results from our 3-D superdroplet simulations with the LDM where the relevant fluctuations in droplet number density have been taken into account; see Appendix A2 for details. The lateral fluctuations are quantified by the relative dispersion $\delta n_{\max}/n_0$. We see that there is a close match between the two lines. This suggests that the superdroplet algorithm is accurate and reproduces the results of the LDM, provided all known corrections are applied to it. It also appears that the additional fluctuations introduced in 3-D compensate for the slight underrepresentation of fluctuations in 1-D.

5. Discussion

Fluctuations play a central role in the LDM. We have therefore used it as a benchmark for our simulation. It turns out that the superdroplet algorithm is able to reproduce the growth histories qualitatively and the distribution of cumulative collision times quantitatively. The role of fluctuations was also investigated by Dziekan and Pawlowska (2017), whose approach to assessing the

fluctuations is different from ours. Instead of analyzing the distribution of cumulative collision times, as we do here, their primary diagnostics is the time $t_{10\%}$, after which 10% of the mass of cloud droplets has reached a radius of $40\,\mu$m. In the LDM, such a time would be infinite, because there is only one droplet that is allowed to grow. They then determined the accuracy with which the value of $t_{10\%}$ is determined. The accuracy increases with the square root of the number of physical droplets, provided that the ratio $N_{\mathrm{p/s}}$ is kept below a limiting value of about 9. For $N_{\mathrm{p/s}} > 9$, they found that there is always a residual error in the value of $t_{10\%}$ that no longer diminishes as they increase the number of physical droplets. They argue that this could be a consequence of introducing unrealistic correlations between different droplet sizes. The nature of such correlations remained, however, unclear. We have demonstrated that, when $N_{\mathrm{p/s}} > 1$, jumps in the growth history tend to occur. Those jumps can lead to shorter cumulative collision times, which could be the source of the residual error they find.

For a given fraction of droplets that first reach a size of $40\,\mu$m, they also determined their average cumulative collision time. They found a significant dependence on the number of physical droplets. This is very different in our case where we just have to make sure that the number of superdroplets is large enough to keep finding collision partners in the simulations. However, as the authors point out, this is a consequence of them having chosen an initial distribution of droplet sizes that has a finite width. This implies that for a larger number of droplets, there is a larger chance that there could be a droplet that is more lucky than for a model with a smaller number of droplets. In our case, by contrast, we always have a well-known number of superdroplets of exactly $12.6\,\mu$m, which avoids the sensitivity on the number of droplets.

The $N_{\mathrm{p/s}} = 9$ limit of Dziekan and Pawlowska (2017) may not be as stringent as originally believed. In this context we need to recall that their criterion for acceptable quality concerned the

relative error of the time in which 10% of the total water has been converted to 40 μm droplets. In our case, we have focussed on the shape of the $P(T)$ curve, especially for small T.

6. Conclusions

We have investigated the growth histories of droplets settling under gravity using superdroplet simulations. The goal was to determine how accurately these simulations represent the fluctuations of the growth histories. This is important because the observed formation time of drizzle-sized droplets is much shorter than the one predicted based on the mean collisional cross section. The work of Telford (1955), Kostinski and Shaw (2005), and Wilkinson (2016) have shown that this discrepancy can be explained by the presence of stochastic fluctuations in the time intervals between droplet collisions. By comparing with the lucky droplet model (LDM) quantitatively, we have shown that the superdroplet simulations can capture fluctuations reasonably well.

An accurate tool to quantify the significance of fluctuations on the growth history of droplets is the distribution of cumulative collision times. The present results have shown that the superdroplet algorithm reproduces the distribution of cumulative collision times that is theoretically expected based on the LDM (approaches I, II, and III). In 3-D, there are additional fluctuations in the system owing to the fact that the mean column density of droplets varies in the horizontal plane. Again, this effect is reproduced by the superdroplet algorithm, where the size distribution is computed from an ensemble with different number densities.

The approximation $\lambda_k \propto r_k^{4/3}$ is not accurate and must be relaxed for a useful benchmark experiment. The superdroplet algorithm demonstrates clear differences between 1-D and 3-D simulations. The broader $P(T)$ distribution can be explained by an extension to any of the approaches I, II, or III that takes horizontal droplet fluctuations into account.

In summary, the superdroplet algorithm appears to take fluctuations reasonably well into account, at least in the context of the problem of coagulation from gravitational settling. Computing the distribution of cumulative collision times in the context of turbulent coagulation would be rather expensive, because one would need to perform many hundreds of fully resolved 3-D simulations. Our study suggests that fluctuations are correctly described for collisions between droplets settling in quiescent fluid, but we do not know whether this conclusion carries over to the turbulent case.

Acknowledgements

This work was supported through the FRINATEK grant 231444 under the Research Council of Norway, SeRC, the Swedish Research Council grants 2012-5797, 2013-03992, and 2017-03865, Formas grant 2014-585, by the University of Colorado through its support of the George Ellery Hale visiting faculty appointment, and by the grant "Bottlenecks for particle growth in turbulent aerosols" from the Knut and Alice Wallenberg Foundation, Dnr. KAW 2014.0048. The simulations were performed using resources provided by the Swedish National Infrastructure for Computing (SNIC) at the Royal Institute of Technology in Stockholm and Chalmers Centre for Computational Science and Engineering (C3SE). This work also benefited from computer resources made available through the Norwegian NOTUR program, under award NN9405K. The source code used for the simulations of this study, the PENCIL CODE, is freely available on `https://github.com/pencil-code/`.

APPENDIX

A1. $P(T)$ for different N_s/N_{grid} and N_d/N_s

This appendix is to demonstrate the statistical convergence of $P(T)$ for different values of N_s/N_{grid} and N_d/N_s. As shown in Figure 15(a), $P(T)$ converges even at $N_s/N_{grid} = 1$. More importantly, Figure 15(b) shows that $P(T)$ is insensitive to N_d/N_s, which suggests that the superdroplet approach can capture the effects of fluctuations regardless of the value of N_d/N_s. This is different from Dziekan and Pawlowska (2017), who found that the approach can represent fluctuations only if $N_d/N_s \leq 9$.

A2. The 3-D LDM

In this appendix, we describe in more detail the 3-D LDM used in Sec. 4d. The usual LDM applies to a given value of the number density. Other columns have somewhat different number densities and therefore also different mean cumulative collision times. The LDM with approaches I–III can be extended to include this effect by computing cases with different number densities and then combining $P(T)$ and normalizing by the $\langle T \rangle$ for the combined $P(T)$. This can be formulated by introducing the column density as

$$\Sigma(x,y) = \int_{z_1}^{z_2} n(x,y,z)\,\mathrm{d}z, \tag{A1}$$

where z_1 and z_2 denote the vertical slab in which the first collision occurs, and using this $\Sigma(x,y)$ as a weighting factor for the 1-D distribution functions $P^{1D}(T)$ to compute the 3-D distribution functions as

$$P^{3D}(T) = \int \Sigma(x,y) P^{1D}(T)\,\mathrm{d}x\,\mathrm{d}y \Big/ \int \Sigma(x,y)\,\mathrm{d}x\,\mathrm{d}y. \tag{A2}$$

Since the first collision matters the most, we choose $z_2 = z_{max}$ (where the lucky droplet is released) and $z_1 = z_{max} - v_2/\lambda_2$ (where it has its first collision).

Our reference model had a number density of $n_0 = 10^8\,\mathrm{m}^{-3}$. We now consider compositions of models with different values, where we include the densities (i) $0.9\times10^8\,\mathrm{m}^{-3}$ and $1.1\times10^8\,\mathrm{m}^{-3}$, as well as (ii) $0.8\times10^8\,\mathrm{m}^{-3}$ and $1.2\times10^8\,\mathrm{m}^{-3}$, and finally also (iii) $0.7\times10^8\,\mathrm{m}^{-3}$ and $1.3\times10^8\,\mathrm{m}^{-3}$. All these compositions have the same mean droplet number density but different distributions around the mean. We first average the distribution function and then normalize with respect to the mean collision time for the ensemble over all columns. The parameters of the resulting distributions are listed in Table 4 for three compositions with different density dispersions. We see that, as we move from composition (i) to compositions (ii) and (iii), the dispersion ($\delta n_{\mathrm{rms}}/n_0$) increases from 0.08 to 0.14 and 0.20, the distribution $P(T)$ extends further to both the left and right. The reference model is listed as (o). Here we give the rms value of the column-averaged densities, $\langle n\rangle_i$, as

$$\delta n_{\mathrm{rms}} = \left[\sum_{i=0}^{N_i}\left(\langle n\rangle_i^2 - n_0^2\right)\right]^{1/2}, \tag{A3}$$

where i denotes the column and N_i is the number of columns. We also give the maximum difference from the average density,

$$\delta n_{\mathrm{max}} = \max_i\left(\langle n\rangle_i - n_0\right), \tag{A4}$$

for families (i) with $N_i = 2$, (ii) with $N_i = 4$, and (iii) with $N_i = 6$. We also list in Table 4 several characteristic times in seconds. The quantity T_{min} is the shortest time in which the lucky droplet reaches $50\,\mu$m, T_{MFT} denotes the value based on MFT, $\langle T(n_{\mathrm{max}})\rangle$ is the mean value based on the column with maximum droplet density and $\langle T\rangle$ is the mean based on all columns. It turns out that for the models of all three families, the value of T_{min} agrees with that obtained solely from the model with the highest density, which is $1.3\times10^8\,\mathrm{m}^{-3}$ for composition (ii), for example.

The quantity $\langle T(n_{\mathrm{max}})\rangle$, i.e., the average time for all of the columns with the largest density, is shorter than the $\langle T\rangle$ for all the columns, especially for composition (iii) where the largest densities

occur. For the model (o), there is only one column, so $\langle T(n_{\max})\rangle$ is the same as $\langle T\rangle$. The value T_{MFT} based on MFT is always somewhat shorter than $\langle T(n_{\max})\rangle$. Finally, we give in Table 4 the ratios $T_{\min}/\langle T\rangle$ and $T_{P=0.01}/\langle T\rangle$, where the subscript $P = 0.01$ indicates the argument of $P(T)$ where the function value is 0.01.

References

Andrejczuk, M., W. W. Grabowski, J. Reisner, and A. Gadian, 2010: Cloud-aerosol interactions for boundary layer stratocumulus in the lagrangian cloud model. *Journal of Geophysical Research: Atmospheres*, **115 (D22)**, n/a–n/a, doi:10.1029/2010JD014248, URL http://dx.doi.org/10.1029/2010JD014248, d22214.

Andrejczuk, M., J. M. Reisner, B. Henson, M. K. Dubey, and C. A. Jeffery, 2008: The potential impacts of pollution on a nondrizzling stratus deck: Does aerosol number matter more than type? *Journal of Geophysical Research: Atmospheres*, **113 (D19)**, n/a–n/a, doi:10.1029/2007JD009445, URL http://dx.doi.org/10.1029/2007JD009445, d19204.

Arabas, A., and S. Shima, 2013: Large-eddy simulations of trade wind cumuli using particle-based microphysics with monte carlo coalescence. *Journal of the Atmospheric Sciences*, **70 (9)**, 2768–2777, doi:10.1175/JAS-D-12-0295.1, URL http://dx.doi.org/10.1175/JAS-D-12-0295.1, http://dx.doi.org/10.1175/JAS-D-12-0295.1.

Baehr, H., and H. Klahr, 2019: The concentration and growth of solids in fragmenting circumstellar disks. *The Astrophysical Journal*, **881 (2)**, 162.

Brdar, S., and A. Seifert, 2018: Mcsnow: A monte-carlo particle model for riming and aggregation of ice particles in a multidimensional microphysical phase space. *J. Adv. Modeling Earth Systems*, **10 (1)**, 187–206.

Drakowska, J., F. Windmark, and C. P. Dullemond, 2014: Modeling dust growth in protoplanetary disks: The breakthrough case. *Astron. & Astrophys.*, **567**, A38, doi:10.1051/0004-6361/201423708, 1406.0870.

Dziekan, P., and H. Pawlowska, 2017: Stochastic coalescence in lagrangian cloud microphysics. *Atmospheric Chemistry and Physics*, **17 (22)**, 13 509–13 520.

Dziekan, P., M. Waruszewski, and H. Pawlowska, 2019: University of warsaw lagrangian cloud model (uwlcm) 1.0: a modern large-eddy simulation tool for warm cloud modeling with lagrangian microphysics. *Geoscientific Model Development*, **12 (6)**, 2587–2606.

Gillespie, D. T., 1972: The stochastic coalescence model for cloud droplet growth. *Journal of the Atmospheric Sciences*, **29 (8)**, 1496–1510.

Grabowski, W. W., 2020: Comparison of Eulerian Bin and Lagrangian Particle-Based Microphysics in Simulations of Nonprecipitating Cumulus. *Journal of Atmospheric Sciences*, **77 (11)**, 3951–3970, doi:10.1175/JAS-D-20-0100.1.

Grabowski, W. W., H. Morrison, S.-I. Shima, G. C. Abade, P. Dziekan, and H. Pawlowska, 2019: Modeling of cloud microphysics: Can we do better? *Bulletin of the American Meteorological Society*, **100 (4)**, 655–672.

Hoffmann, F., T. Yamaguchi, and G. Feingold, 2019: Inhomogeneous mixing in lagrangian cloud models: Effects on the production of precipitation embryos. *Journal of the Atmospheric Sciences*, **76 (1)**, 113–133.

Johansen, A., M.-M. Mac Low, P. Lacerda, and M. Bizzarro, 2015: Growth of asteroids, planetary embryos, and kuiper belt objects by chondrule accretion. *Science Advances*, **1 (3)**, e1500 109.

Johansen, A., A. N. Youdin, and Y. Lithwick, 2012: Adding particle collisions to the formation of asteroids and kuiper belt objects via streaming instabilities. *Astron, Astroph.*, **537**, A125.

Jokulsdottir, T., and D. Archer, 2016: A stochastic, lagrangian model of sinking biogenic aggregates in the ocean (slams 1.0): model formulation, validation and sensitivity. *Geoscientific Model Development*, **9 (4)**, 1455–1476.

Kobayashi, H., K. Isoya, and Y. Sato, 2019: Importance of giant impact ejecta for orbits of planets formed during the giant impact era. *The Astrophysical Journal*, **887 (2)**, 226.

Kostinski, A. B., and R. A. Shaw, 2005: Fluctuations and luck in droplet growth by coalescence. *Bull. Am. Met. Soc.*, **86**, 235–244.

Lamb, D., and J. Verlinde, 2011: *Growth by collection*, 380–414. Cambridge University Press, doi:10.1017/CBO9780511976377.010.

Li, X.-Y., A. Brandenburg, N. E. L. Haugen, and G. Svensson, 2017: Eulerian and lagrangian approaches to multidimensional condensation and collection. *J. Adv. Modeling Earth Systems*, **9**, 1116–1137.

Li, X.-Y., A. Brandenburg, G. Svensson, N. E. Haugen, B. Mehlig, and I. Rogachevskii, 2018: Effect of turbulence on collisional growth of cloud droplets. *Journal of the Atmospheric Sciences*, **75 (10)**, 3469–3487.

Li, X.-Y., A. Brandenburg, G. Svensson, N. E. Haugen, B. Mehlig, and I. Rogachevskii, 2020: Condensational and collisional growth of cloud droplets in a turbulent environment. *Journal of the Atmospheric Sciences*, **77 (1)**, 337–353.

Li, X.-Y., and L. Mattsson, 2020: Coagulation of inertial particles in supersonic turbulence. *arXiv preprint arXiv:2002.12172*.

Li, X.-Y., G. Svensson, A. Brandenburg, and N. E. L. Haugen, 2019: Cloud-droplet growth due to supersaturation fluctuations in stratiform clouds. *Atmospheric Chemistry and Physics*, **19 (1)**, 639–648, doi:10.5194/acp-19-639-2019, URL https://www.atmos-chem-phys.net/19/639/2019/.

Naumann, A. K., and A. Seifert, 2015: A lagrangian drop model to study warm rain microphysical processes in shallow cumulus. *Journal of Advances in Modeling Earth Systems*, **7 (3)**, 1136–1154, doi:10.1002/2015MS000456, URL http://dx.doi.org/10.1002/2015MS000456.

Naumann, A. K., and A. Seifert, 2016: Recirculation and growth of raindrops in simulated shallow cumulus. *Journal of Advances in Modeling Earth Systems*, n/a–n/a, doi:10.1002/2016MS000631, URL http://dx.doi.org/10.1002/2016MS000631.

Nesvornỳ, D., R. Li, A. N. Youdin, J. B. Simon, and W. M. Grundy, 2019: Trans-neptunian binaries as evidence for planetesimal formation by the streaming instability. *Nature Astronomy*, **3 (9)**, 808–812.

Onishi, R., K. Matsuda, and K. Takahashi, 2015: Lagrangian tracking simulation of droplet growth in turbulence–turbulence enhancement of autoconversion rate. *Journal of the Atmospheric Sciences*, **72 (7)**, 2591–2607.

Ormel, C., D. Paszun, C. Dominik, and A. Tielens, 2009: Dust coagulation and fragmentation in molecular clouds-i. how collisions between dust aggregates alter the dust size distribution. *Astronomy & Astrophysics*, **502 (3)**, 845–869.

Patterson, R. I., and W. Wagner, 2012: A stochastic weighted particle method for coagulation–advection problems. *SIAM Journal on Scientific Computing*, **34 (3)**, B290–B311.

Poon, S. T., R. P. Nelson, S. A. Jacobson, and A. Morbidelli, 2020: Formation of compact systems of super-earths via dynamical instabilities and giant impacts. *Monthly Notices of the Royal Astronomical Society*, **491 (4)**, 5595–5620.

Pruppacher, H. R., and J. D. Klett, 1997: *Microphysics of clouds and precipitation, 2nd edition*. Kluwer Academic Publishers, Dordrecht, The Nederlands, 954p.

Riechelmann, T., Y. Noh, and S. Raasch, 2012: A new method for large-eddy simulations of clouds with lagrangian droplets including the effects of turbulent collision. *New Journal of Physics*, **14 (6)**, 065 008, URL http://stacks.iop.org/1367-2630/14/i=6/a=065008.

Ros, K., and A. Johansen, 2013: Ice condensation as a planet formation mechanism. *Astronomy & Astrophysics*, **552**, A137.

Ros, K., A. Johansen, I. Riipinen, and D. Schlesinger, 2019: Effect of nucleation on icy pebble growth in protoplanetary discs. *Astronomy & Astrophysics*, **629**, A65.

Saffman, P. G., and J. S. Turner, 1956: On the collision of drops in turbulent clouds. *J. Fluid Mech.*, **1**, 16–30, doi:10.1017/S0022112056000020.

Saito, I., and T. Gotoh, 2018: Turbulence and cloud droplets in cumulus clouds. *New Journal of Physics*, **20 (2)**, 023 001.

Sato, Y., S.-i. Shima, and H. Tomita, 2017: A grid refinement study of trade wind cumuli simulated by a lagrangian cloud microphysical model: the super-droplet method. *Atmospheric Science Letters*, **18 (9)**, 359–365.

Shima, S., K. Kusano, A. Kawano, T. Sugiyama, and S. Kawahara, 2009: The super-droplet method for the numerical simulation of clouds and precipitation: a particle-based and proba-

bilistic microphysics model coupled with a non-hydrostatic model. *Quart. J. Roy. Met. Soc.*, **135**, 1307–1320, doi:10.1002/qj.441, physics/0701103.

Sokal, A., 1997: *Monte Carlo Methods in Statistical Mechanics: Foundations and New Algorithms*. Boston: Springer.

Sölch, I., and B. Kärcher, 2010: A large-eddy model for cirrus clouds with explicit aerosol and ice microphysics and lagrangian ice particle tracking. *Quarterly Journal of the Royal Meteorological Society*, **136 (653)**, 2074–2093.

Telford, J. W., 1955: A new aspect of coalescence theory. *Journal of Meteorology*, **12 (5)**, 436–444.

Unterstrasser, S., F. Hoffmann, and M. Lerch, 2017: Collection/aggregation algorithms in lagrangian cloud microphysical models: rigorous evaluation in box model simulations. *Geoscientific Model Development*, **10 (4)**, 1521–1548, doi:10.5194/gmd-10-1521-2017, URL https://www.geosci-model-dev.net/10/1521/2017/.

Wilkinson, M., 2016: Large deviation analysis of rapid onset of rain showers. *Phys. Rev. Lett.*, **116**, 018 501, doi:10.1103/PhysRevLett.116.018501, URL http://link.aps.org/doi/10.1103/PhysRevLett.116.018501.

Yang, C.-C., and Z. Zhu, 2020: Morphological signatures induced by dust back reaction in discs with an embedded planet. *Monthly Notices of the Royal Astronomical Society*, **491 (4)**, 4702–4718.

Zsom, A., and C. P. Dullemond, 2008: A representative particle approach to coagulation and fragmentation of dust aggregates and fluid droplets. *Astron. Astrophys.*, **489 (2)**, 931–941.

666 Zsom, A., C. Ormel, C. Güttler, J. Blum, and C. Dullemond, 2010: The outcome of protoplan-
667 etary dust growth: pebbles, boulders, or planetesimals?-ii. introducing the bouncing barrier.
668 *Astronomy & Astrophysics*, **513**, A57.

LIST OF TABLES

TABLE 1. Definition of variables in superdroplet algorithm.

N_{s}	Number of 'superdroplets'
$N_{\mathrm{p/s}}$	Number of droplets in a superdroplet
$N_{\mathrm{p}} = N_{\mathrm{p/s}} N_{\mathrm{s}}$	Total number of droplets (or particles)
N_{real}	number of independent simulations (realizations)

TABLE 2. Moments of $X = \ln(T/\langle T\rangle)$ computed from 10^{10} realizations for different values of r_* (in μm]), and different prescriptions of $r_{\rm A}$ and $r_{\rm B}$. The corresponding values of $T_k^{\rm MFT}$ are also given and are normalized to unity for $r_{\rm A} \neq r_k \neq r_{\rm B}$ with $r_* \geq 50\,\mu$m.

r_*	$r_{\rm A}$	$r_{\rm B}$	$T_k^{\rm MFT}$	$\langle X\rangle$	$\sigma(X)$	skew X	kurt X
—	—	r_k	0.67	−0.020	0.21	0.22	0.08
—	r_k	r_k	1.49	−0.033	0.25	0.25	0.05
—	—	—	1	−0.040	0.28	0.34	0.10
40	—	—	0.99	−0.041	0.28	0.33	0.09
30	—	—	0.93	−0.046	0.30	0.28	0.05
20	—	—	0.79	−0.063	0.35	0.18	−0.04
10	—	—	0.34	−0.111	0.47	0.16	−0.17

TABLE 3. Comparison of the moments of $X = \ln(T/\langle T \rangle)$ for approaches I–III.

Approach	$\langle X \rangle$	$\sigma(X)$	skew X	kurt X
I	-0.040	0.279	0.34	0.10
II	-0.039	0.275	0.35	0.11
III	-0.040	0.279	0.34	0.11

681 TABLE 4. Results for approach II using 30,000 realization showing the effects of lateral density fluctuations
682 in 3-D, and comparison with MFT.

Composition	$\delta n_{\rm rms}/n_0$	$\delta n_{\rm max}/n_0$	$T_{\rm min}$ [s]	$T_{\rm MFT}$ [s]	$\langle T(n_{\rm max})\rangle$ [s]	$\langle T\rangle$ [s]	$T_{\rm min}/\langle T\rangle$	$T_{P=0.01}/\langle T\rangle$
(0)	0	0	782	1969	2117	2117	0.37	0.44
(i)	0.08	0.10	795	1790	1923	2126	0.37	0.42
(ii)	0.14	0.20	767	1641	1758	2155	0.36	0.40
(iii)	0.20	0.30	631	1515	1628	2203	0.29	0.36

LIST OF FIGURES

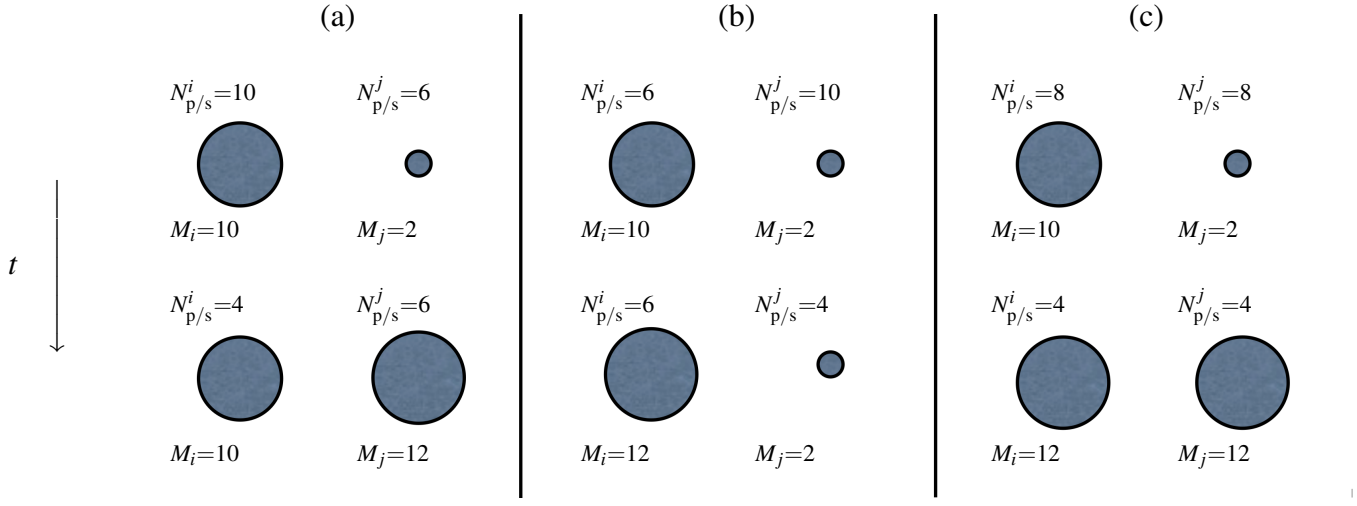

722 FIG. 1. Collision outcomes when two superdroplets collide and droplet collisions occur. Time increases
723 downward, as indicated by the arrow. Superdroplet i contains $N^i_{\mathrm{p/s}}$ large droplets of mass M_i, superdroplet j
724 contains $N^j_{\mathrm{p/s}}$ small droplets of mass $M_j < M_i$.

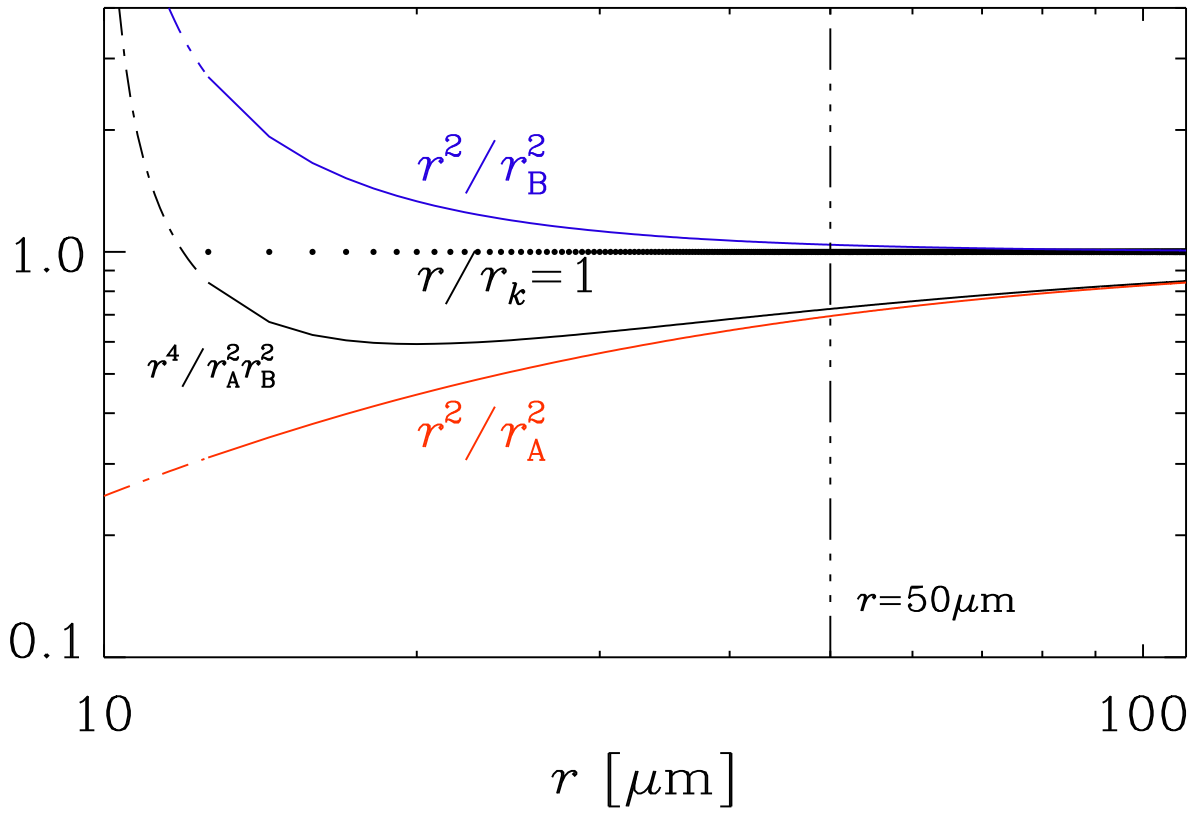

725 FIG. 2. Contributions to the two correction factors r^2/r_A^2 (red) and r^2/r_B^2 (blue), as well as their product. The
726 discrete radii r_k for $k \geq 2$ are shown in a horizontal line of dots. The vertical dash-triple-dotted lines denote the
727 radius $r = 50\,\mu$m.

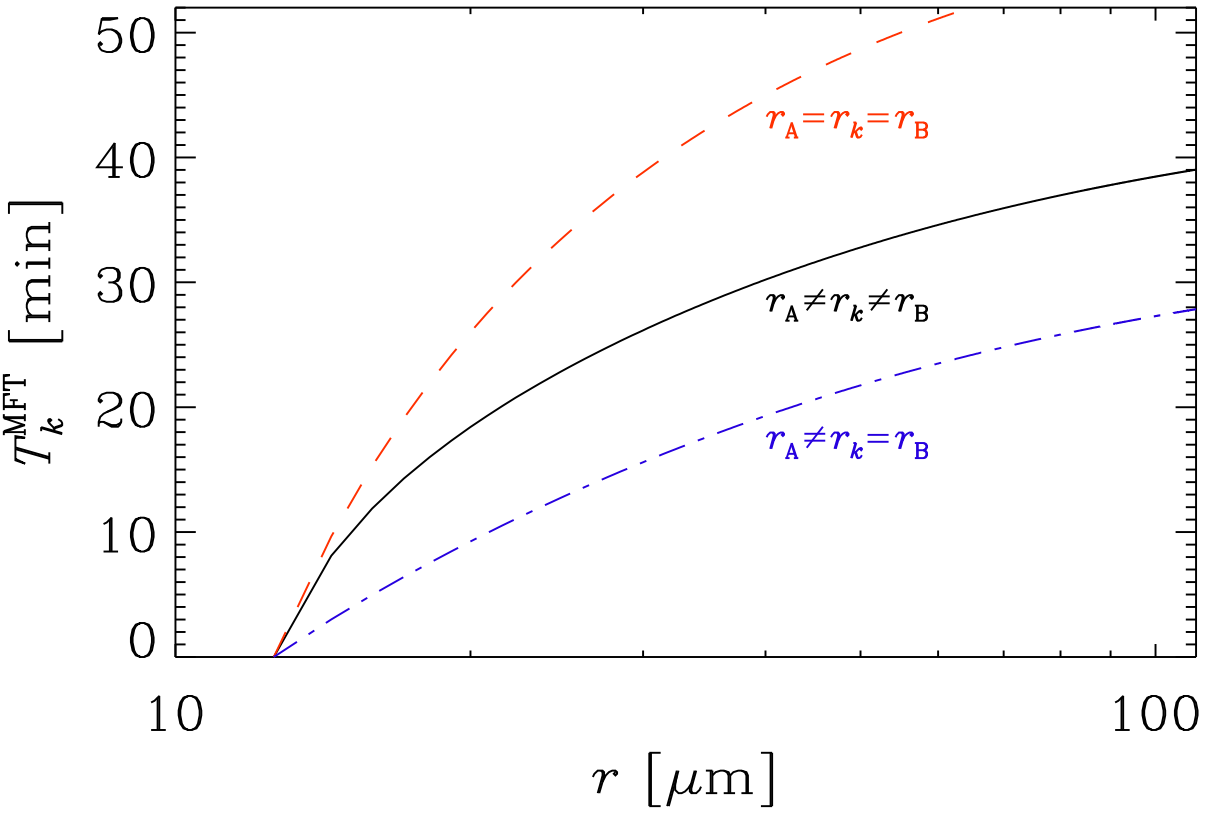

728 FIG. 3. Cumulative mean collision times, T_k^{MFT}, for $r_\mathrm{A} \neq r_k \neq r_\mathrm{B}$ (solid black line), compared with the
729 approximations $r_\mathrm{A} = r_\mathrm{B} = r_k$ (red dashed line) and only $r_\mathrm{B} = r_k$ (blue dash-dotted line).

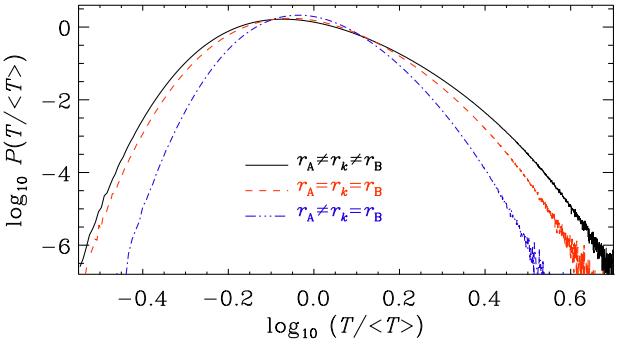

730 FIG. 4. Comparison of $P(T)$ in a double-logarithmic representation for the LDM appropriate to our benchmark
731 (black solid line) with various approximations where $r_\mathrm{A} = r_\mathrm{B} = r_k$ (red dashed line) along with a case where
732 only $r_\mathrm{B} = r_k$ is assumed (blue dash-dotted line).

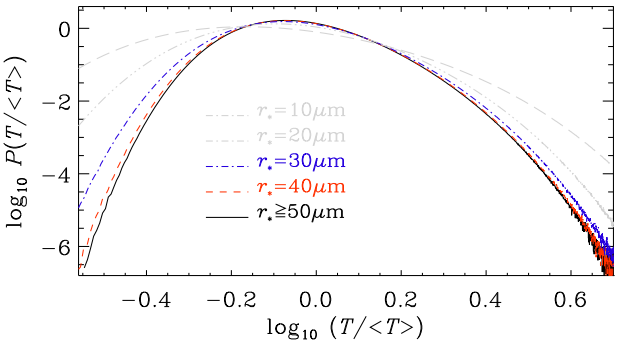

733 FIG. 5. Comparison of $P(T)$ in a double-logarithmic representation for the LDM for $r_* = 40\,\mu$m and $30\,\mu$m
734 using $r_A \neq r_k \neq r_B$. The black line agrees with that in Figure 4, and the two gray lines refer to the cases with
735 $r_* = 20\,\mu$m and $10\,\mu$m.

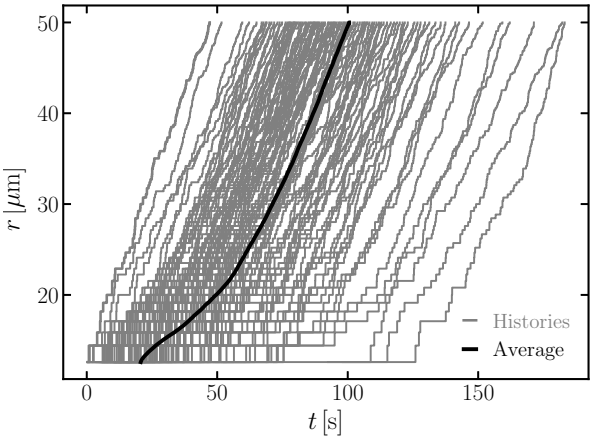

736 FIG. 6. 98 growth histories of lucky droplets obtained from 98 independent superdroplet simulations, as
737 described in the text. All superdroplets have initially the same number of droplets, $N_{p/s} = 1$ with $N_s = 256$. The
738 mean number density of droplets is $n_0 = 2.28 \times 10^9\,\mathrm{m}^{-3}$. The fat solid line shows the average time for each
739 radius.

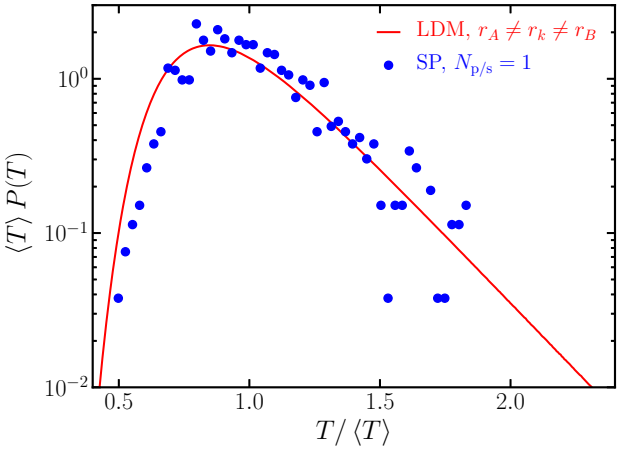

FIG. 7. $P(T)$ obtained with the superdroplet algorithm (blue dots), the LDM with $r_{\mathrm{A}} \neq r_k \neq r_{\mathrm{B}}$ (red solid line).

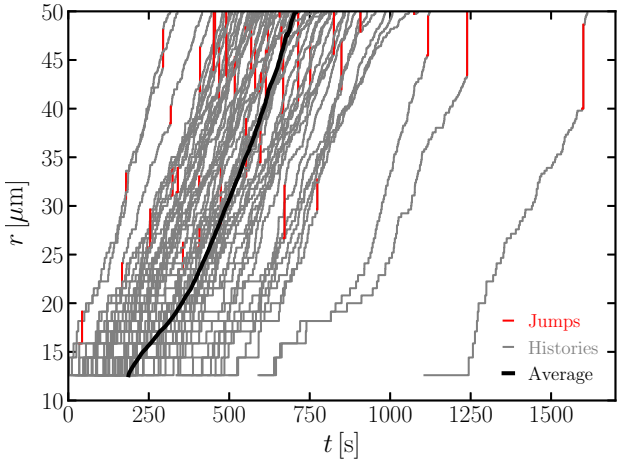

740 FIG. 8. Same as Figure 6 but with initial condition $N_{\mathrm{p/s}} = 2$ initially. Note the occurrence of jumps, indicated
741 in red.

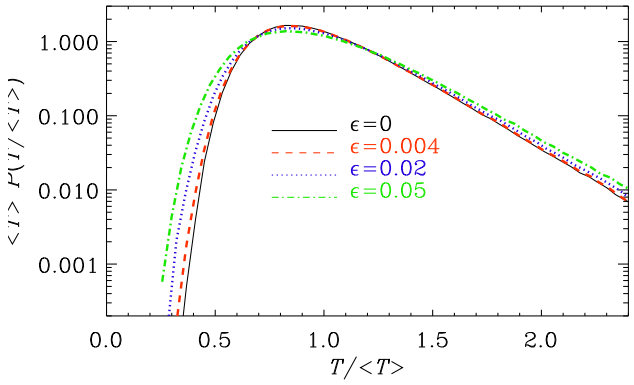

742 FIG. 9. Comparison of models with $\varepsilon = 0$ (no jumps), 0.004 (the value expected for the simulations), 0.02,
743 and 0.05.

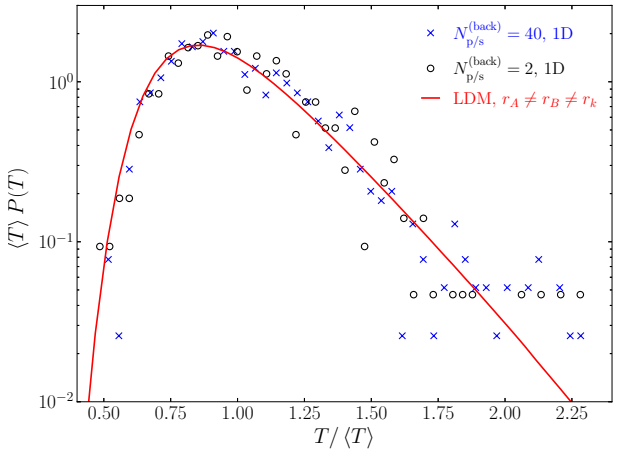

744 FIG. 10. Simulations with initially $N_{\rm p/s}^{\rm (back)} = 40$ (blue crosses) and $N_{\rm p/s}^{\rm (back)} = 2$ (black circles), and $N_{\rm p/s}^{\rm (luck)} = 2$
745 in both cases. The red line denotes the relevant LDM.

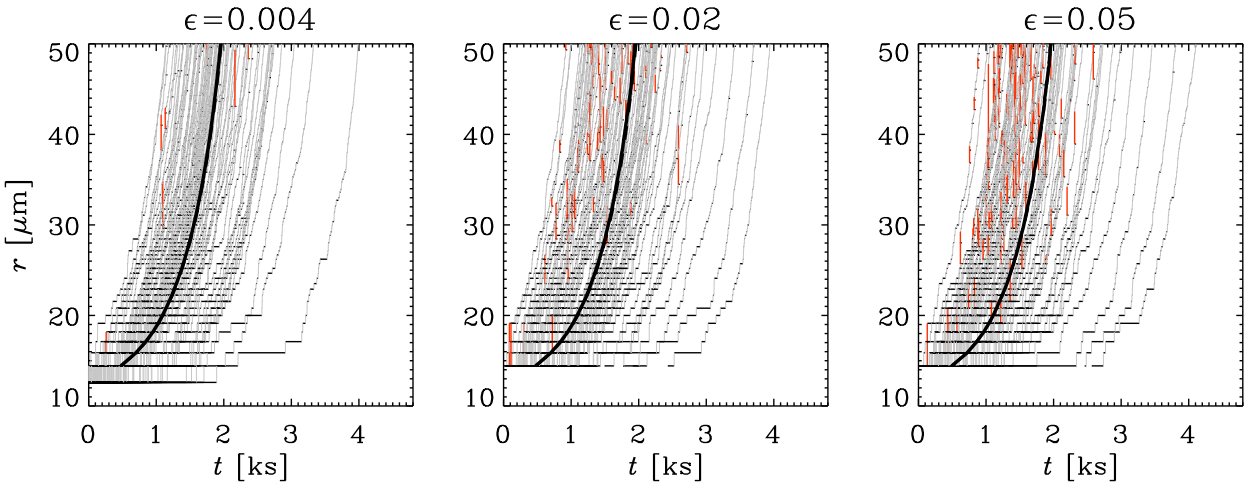

FIG. 11. Growth histories for $\varepsilon = 0.004$ (very few jumps, relevant to the simulations of Figure 7), as well as $\varepsilon = 0.02$, and 0.05, where jumps are more frequent. The thick solid line gives the average collision time and cannot be distinguished from that of MFT, which is shown as a thick dotted line.

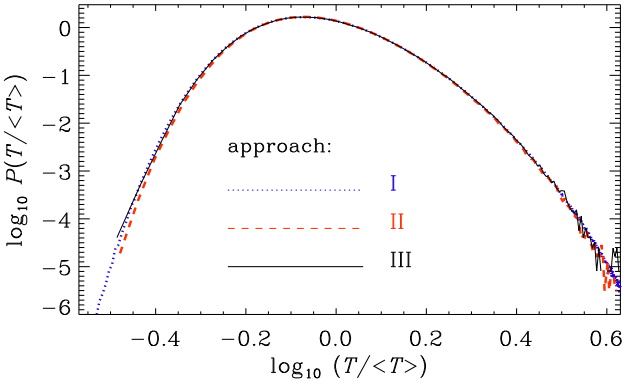

FIG. 12. Comparison of $P(T)$ for approaches I, II, and III.

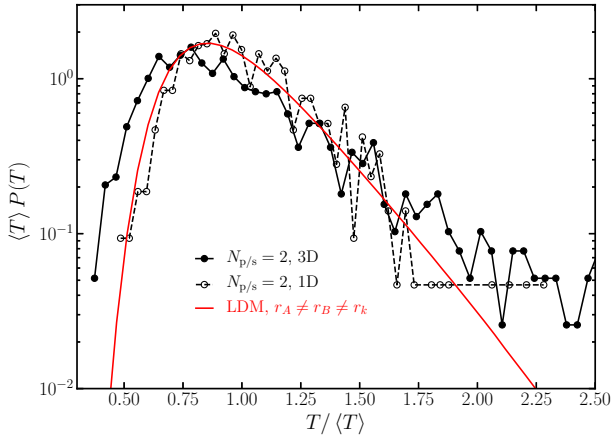

749 FIG. 13. Comparison of the 3-D case (solid black line) with the 1-D case (dotted black line) with $N_{\mathrm{p/s}} = 2$.
750 The red curve shows the result for the LDM with $r_{\mathrm{A}} \neq r_{\mathrm{B}} \neq r_k$.

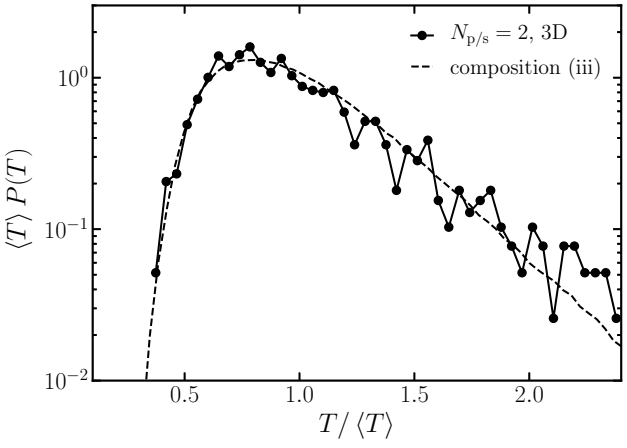

751 FIG. 14. Comparison between the 3-D superdroplet simulation of Figure 13 and approach II evaluated with a
752 dispersion of $\delta n_{\mathrm{max}}/n_0 = 0.2$, corresponding to composition (iii); see Table 4 for details.

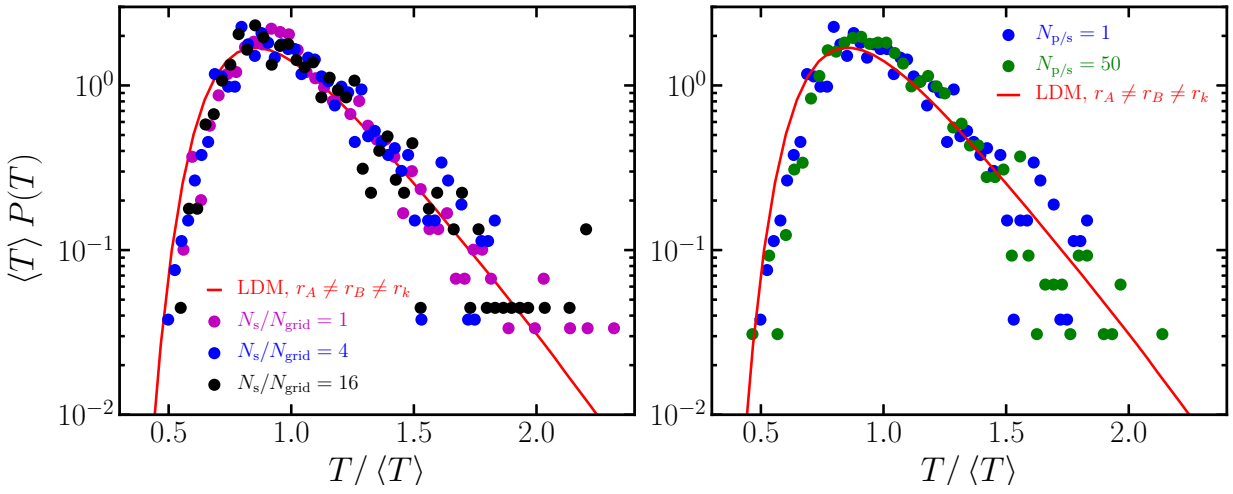

753 FIG. 15. Comparison of $P(T)$ for different $N_s/N_{\rm grid}$ with fixed $N_{p/s} = 1$ (left panel) and for different $N_{p/s}$ with
754 fixed $N_s/N_{\rm grid} = 4$. Same simulation as in Figure 7(a).